

Modeling the Neuromuscular Control System of an Octopus Arm ^{*}

Tixian Wang ^{*,**} Udit Halder ^{**} Ekaterina Gribkova ^{***}
Mattia Gazzola ^{****,†} Prashant G. Mehta ^{*,**}

^{*} Department of Mechanical Science and Engineering

^{**} Coordinated Science Laboratory

^{***} Neuroscience Program

^{****} National Center for Supercomputing Applications

[†] Carl R. Woese Institute for Genomic Biology

University of Illinois at Urbana-Champaign, Champaign, IL 61820 USA

Corresponding e-mail: udit@illinois.edu

Abstract: The octopus arm is a neuromechanical system that involves a complex interplay between peripheral nervous system (PNS) and arm musculature. This makes the arm capable of carrying out rich maneuvers. In this paper, we build a model for the PNS and integrate it with a muscular soft octopus arm. The proposed neuromuscular architecture is used to qualitatively reproduce several biophysical observations in real octopuses, including curled rest shapes and target-directed arm reaching motions. Two control laws are proposed for target-oriented arm motions, and their performance is compared against a benchmark. Several analytical results, including rest-state characterization and stability properties of the proposed control laws, are provided.

Keywords: Octopus; Neuromuscular control; Cable equation; Sensorimotor control; Feedback control; Lyapunov stability; Bend propagation

1. INTRODUCTION

The octopus arm is a muscular hydrostatic limb characterized by virtually infinite degrees of freedom and extreme flexibility (Kennedy et al., 2020; Levy et al., 2017). Octopus arm movements have been widely studied by biologists over the past few decades (Gutfreund et al., 1998; Sumbre et al., 2001; Yekutieli et al., 2005a; Hanassy et al., 2015). Efficient control of such flexible appendages is challenging due to the distributed nature of sensing and motor control. Several control strategies have been proposed for octopus arm movements, including stiffening wave actuation (Yoram et al., 2002; Yekutieli et al., 2005a,b; Wang et al., 2022a), energy shaping control (Chang et al., 2020, 2021, 2022), optimal control (Cacace et al., 2019; Wang et al., 2021), and sensory feedback control (Wang et al., 2022b). However, these studies remain at muscle actuation level, lacking integration with the peripheral nervous system (PNS).

Beyond octopus arms, neural control has been studied over decades for various animals and applications in robotics, such as neural modeling from biological studies (Ekeberg, 1993; Matsuoka, 1984), robot and actuators (Ijspeert et al., 2007; Aydin et al., 2019), neuromorphic control (Folghera et al., 2019; Polykretis et al., 2022), central pattern generator for locomotion (Sfakiotakis and Tsakiris, 2007; Liu et al., 2008; Wang et al., 2020), etc.

The main contribution of this paper lies in the derivation of a simple PNS model and in its assimilation within the arm musculature. The coupled neuromuscular system is then shown to recapitulate a range of experimentally observed behaviors.

1.1 Biological background

1) Anatomy: Neural architecture. The arm PNS includes a large axial nerve cord (ANC) running along the length of the arm (Fig. 1(a)), and with a brachial ganglion and sucker ganglion for each sucker of the arm (Rowell, 1963; Matzner et al., 2000). It is estimated that *Octopus vulgaris* has around 300 suckers arranged in two rows along each arm, with about 350 million neurons in the PNS of all eight arms (Young, 1971; Wells, 1978). The sucker ganglia receive chemosensory information (Graziadei and Gagne, 1976; Mather, 2021), whereas the brachial ganglia receive local proprioceptive information (Grasso, 2014) and send motor commands along numerous nerve roots to the musculature of the arm (Matzner et al., 2000). Each muscle cell is intricately innervated by motoneurons for efficient and independent motor control (Matzner et al., 2000; Nesher et al., 2019). However, the exact neural circuitry and its functioning for controlling arm movements remain elusive to researchers.

Musculature. The ANC is surrounded by densely packed muscles which are broadly divided into three categories – transverse, longitudinal, and oblique (Kier and Stella, 2007; Kier, 2016). Transverse muscles are oriented orthogonally to the axial direction and are responsible for extending the arm. Longitudinal muscles run parallel to the ANC and their contractions bend the arm. Finally, oblique muscles are arranged in a helical fashion, making the arm twist upon contraction.

* We gratefully acknowledge financial support from ONR MURI N00014-19-1-2373, and NSF EFRI C3 SoRo #1830881. We also acknowledge computing resources provided by the Extreme Science and Engineering Discovery Environment (XSEDE), which is supported by National Science Foundation grant number ACI-1548562, through allocation TG-MCB190004.

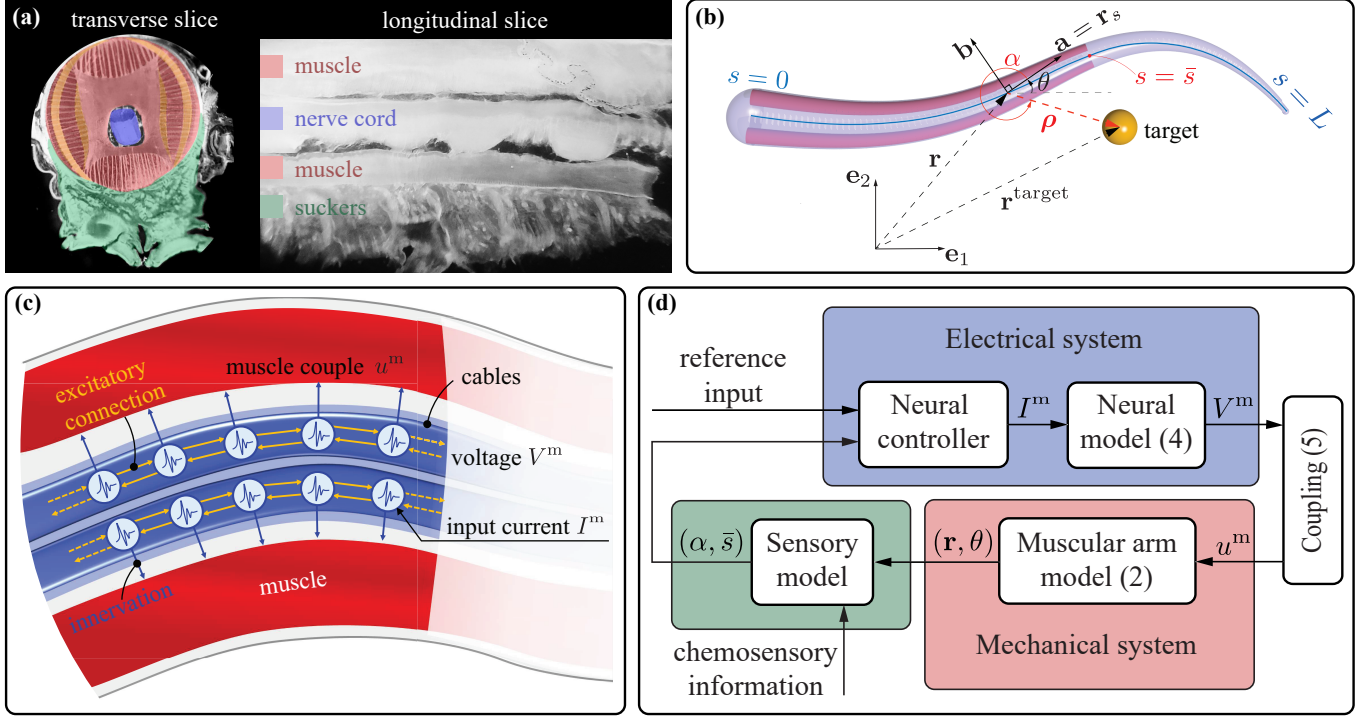


Fig. 1. (a) Physiological cross sections of an *Octopus rubescens* arm. The muscles are color coded in red, the nerve cord is color coded in blue, and the suckers are color coded in green. (b) Schematic of a planar octopus arm with a static target. The sensory information are the bearing α and the arc-length \bar{s} of the closest point to the target. (c) Neuromuscular control architecture. The axial nerve cord is modeled by two electrical cables. (d) A block diagram for the neuromuscular control system with sensing.

2) Behavioral observations

a) *Curled rest state*: Octopus arms tend to curl and form spirals, particularly when at rest (Packard and Sanders, 1971; Mather, 1998), exposing suckers outwardly as shown in Fig. 2(a). This curling behavior may be beneficial for several biophysical reasons. Examples range from protecting the arm from predators, environmental awareness owing to large number of exposed suckers, or providing an efficient initial state for arm reaching motions. Notably, curling at rest seems to persist even without input from the central nervous system (CNS), as observed in isolated arms (Fig. 2(a)). Mechanically, arm curling at rest may involve inherent tensions of the arm muscle groups (Di Clemente et al., 2021).

b) *Goal-directed arm motions*: One of the most common octopus arm motions involves bend propagation wherein the arm creates a bend at the base and actively propagates it along the length of the arm through traveling waves of muscle actuations (Gutfreund et al., 1998; Sumbre et al., 2001; Hanassy et al., 2015). This reaching motion persists in severed arms (Sumbre et al., 2001), suggesting that its motor program could be encoded in the arm PNS as a motion primitive. Fig. 3(a) showcases video frames from one such reaching motion where the curling at the tip is also visible.

1.2 Contributions

This paper is a continuation of our previous work (Chang et al., 2021; Wang et al., 2022a,b) on control strategies for soft arms modeled via Cosserat rod theory (Antman, 1995; Gazzola et al., 2018). The primary contributions of this work are the following.

1) Modeling of the neuronal architecture: A mathematical abstraction of the arm PNS is proposed. Continuum neuronal activity is captured using cable theory (Tuckwell, 1988) and neuromuscular control is in the form of distributed current inputs to the neurons. The coupling between neural and muscular systems, through muscle innervation, is also modeled. This yields a compact description of the soft arm in a system-theoretic manner.

2) Analysis of the neuromuscular control system:

a) *Characterizing the rest state*: An analysis of equilibria of the coupled arm dynamics is provided to show that different curled rest shapes can be obtained. A qualitative comparison is provided between numerical results and biological observations.

b) *Control problem*: Two control laws are proposed for the neuromuscular control system and are shown to accomplish the task of reaching a stationary target. Stability analyses are provided for the same.

The rest of the paper is organized as follows. In Sec. 2, we introduce the proposed neuromuscular control architecture. In Sec. 3, we analyze the arm rest state and describe the neuromuscular control laws for the reaching problem. We provide simulation results in Sec. 4 and conclude in Sec. 5.

2. MODELING

A neuromuscular octopus arm is comprised of several components, including arm musculature, peripheral nervous system, the coupling between the neural (electrical) and the muscular (mechanical) subsystems, and sensing, as shown in Fig. 1(d).

In the rest of this section, we provide models for each of these components.

2.1 Muscular arm

A soft octopus arm is modeled as a planar Cosserat rod (Antman, 1995; Chang et al., 2020, 2021). In this paper, we consider an inextensible and unshearable rod (Kirchhoff rod) for simplicity of exposition. Let $\{\mathbf{e}_1, \mathbf{e}_2\}$ denote a fixed orthonormal basis for the two-dimensional laboratory frame. The independent variables are time $t \in \mathbb{R}$ and arc-length $s \in [0, L]$, where L is the length of the rod (see Fig. 1(b)). The subscripts $(\cdot)_t$ and $(\cdot)_s$ denote partial derivatives with respect to t and s , respectively.

The position vector of the centerline is denoted by $\mathbf{r}(s, t) \in \mathbb{R}^2$ and the angle $\theta(s, t) \in [0, 2\pi)$ describes the material frame spanned by the orthonormal basis $\{\mathbf{a}, \mathbf{b}\}$, where $\mathbf{a} = \cos \theta \mathbf{e}_1 + \sin \theta \mathbf{e}_2$, $\mathbf{b} = -\sin \theta \mathbf{e}_1 + \cos \theta \mathbf{e}_2$. The kinematics of the rod are given by

$$\mathbf{r}_s = \begin{pmatrix} \cos \theta \\ \sin \theta \end{pmatrix} = \mathbf{a}, \quad \theta_s = \kappa \quad (1)$$

where κ is the curvature of the centerline. The dynamics are described by the set of partial differential equations (Antman, 1995; Gazzola et al., 2018; Chang et al., 2021)

$$\begin{aligned} (\varrho A \mathbf{r}_t)_t &= (\mathbf{Qn})_s - \zeta \mathbf{r}_t + \mathbf{f}^{\text{drag}} \\ (\varrho I \theta_t)_t &= (EI \kappa)_s + n_2 - \zeta \theta_t + u_s \end{aligned} \quad (2)$$

where ϱ is density, A is the cross sectional area, $\mathbf{Q} = [\mathbf{a} \ \mathbf{b}]$ is a planar rotation matrix, and $\zeta > 0$ is a damping coefficient which models viscoelastic dissipation within the arm. For a linearly elastic arm, $\mathbf{n} = n_1 \mathbf{a} + n_2 \mathbf{b}$ and $EI \kappa$ are internal passive forces and couples, where E is the Young's modulus and I is the second moment of area of the cross section. The effect of drag forces due to the surrounding fluid environment is captured by \mathbf{f}^{drag} , details of which can be found in (Wang et al., 2022b).

In this paper, we only consider two longitudinal muscles (top (t) and bottom (b), see Fig. 1(b)). Since the arm is assumed to be inextensible and unshearable, we simply model muscle actuations as internal couples on the arm. Let u^t and u^b denote the muscle couples for the top and bottom longitudinal muscles, respectively. Then the total active muscle couple u in (2) is calculated as $u = u^b - u^t$. Additional details on muscle modeling are found in (Chang et al., 2021). Combined with the passive elastic response, the total internal couple is then $m = EI \kappa + u$. Finally, the dynamics (2) are accompanied by a fixed-free boundary condition

$$\mathbf{r}(0, t) = 0, \quad \theta(0, t) = 0, \quad \mathbf{n}(L, t) = 0, \quad m(L, t) = 0 \quad (3)$$

2.2 Peripheral nervous system (PNS)

Muscle contraction control inputs are provided by the underlying electrical activity of neurons. The first mathematical abstraction for an excitable neural media was given by Hodgkin and Huxley (Hodgkin and Huxley, 1952) to describe how the membrane potential or voltage evolves and propagates in a squid giant axon. Along with the membrane potential, the Hodgkin-Huxley model contains three other variables to capture the effects of sodium (Na^+), potassium (K^+), and leakage currents in the action potential dynamics. In the following decades, a wide range of simplified mathematical models were

proposed, a summary of which can be found in (Izhikevich, 2007).

The musculature model in this paper considers two longitudinal muscles independently controlled by the PNS, whose central component is the axial nerve cord (ANC). We model the ANC by two long cylindrical nerves, referred to here as ‘cables’ (see Fig. 1(c)). We model the neural activity of these nerves after the cable theory (Rall, 1962; Tuckwell, 1988) which is a simplified model for one-dimensional excitable media. Each of the two cables is characterized by its distributed membrane voltage $V^m(s, t)$ and a recovery or adaptation variable $W^m(s, t)$, where $m \in \{t, b\}$. The dynamics of such a cable are expressed as the following partial differential equations

$$(\tau V^m)_t = \lambda^2 V_{ss}^m - V^m - W^m + I^m \quad (4a)$$

$$(\tilde{\tau} W^m)_t = -W^m + bg(V^m) \quad (4b)$$

where τ is a time constant, λ is a length constant, $\tilde{\tau}$ is the adaptation rate, and the function $g(x) = \max(x, 0)$ describes the output property of neurons (ReLU). The recovery variable W^m captures the effect of neuron ‘fatigue’ or self-inhibition and b is the adaptation strength (Matsuoka, 1984). Intuitively, the adaptation decreases the effective length constant leading to a faster decaying (in s) neural activity (see discussions in Sec. 4.1). Finally, the term $I^m(s, t)$ denotes the total stimulus current which are produced by the local neural circuitry contained in the ganglia. Since the details of such circuitries are not fully known, we model their net effect by the current inputs to the cables. Therefore the variables I^m are considered to be the control inputs for the arm neuromuscular control system (Fig. 1(d)). Context dependent boundary conditions for the voltage equation (4a) are discussed in Sec. 3.

Remark 1. Notice that on the right hand side of (4a), the linear term $(-V^m)$ is chosen here for simplicity (Matsuoka, 1984). However, other forms have been studied and can be incorporated into our model. For example, the Fitzhugh-Nagumo model (FitzHugh, 1961; Nagumo et al., 1962) uses a cubic term $V^m - \frac{1}{3}(V^m)^3$. Moreover, mutual inhibition has also been studied for models of central pattern generators in octopus arms (Tian and Lu, 2015), a topic we postpone for future studies.

Remark 2. In cable theory, the length constant λ depends on the radius of the cable (Koch, 1984). However, measurements in octopus suggest that the cross sectional area of the nerve cord does not decrease significantly, even though the arm tapers toward the tip (Kier and Stella, 2007). For this reason, we take λ to be a constant.

2.3 Coupling – from neural activity to muscle contractions

The neural activity or the cable voltages are responsible for instructing the muscles to contract through motorneuron innervations. The unique neuromuscular system of the octopus arm shows the lack of short-term synaptic plasticity and post-synaptic inhibition in the neuromuscular junction, which suggests an approximately linear transformation of motor neuronal activity into muscular activation (Matzner et al., 2000; Neshor et al., 2020). We model the coupling between the voltage level and the resulting muscle couple using an activation function $\sigma(\cdot) : \mathbb{R} \mapsto [0, 1]$ as follows

$$u^m(s, t) = c(s) \sigma(V^m(s, t)) \quad (5)$$

where $c(s) > 0$ is the maximum couple a muscle can exert along the arm. The activation function $\sigma(\cdot)$ behaves like a saturation function, i.e. it remains close to zero for low voltages,

then increases approximately linearly, and finally saturates to one for high voltages, reflecting the physical limits of muscles. The explicit formula for $\sigma(\cdot)$ is provided in Sec. 4. Further details of the excitation-contraction dynamics for skeletal muscles can be found in (Hatzel, 1977; Audu and Davy, 1985).

2.4 Sensing

Biological experiments suggest that octopuses use various sensory information, ranging from visual, chemical to proprioceptive, to carry out various manipulation tasks, including reaching to a target (Gutnick et al., 2020; Mather, 2021). Based on these evidences, we introduced a simplified sensory model in our recent work (Wang et al., 2022b). The sensory model assumes that the arm has access to the bearing angle α and the location ($s = \bar{s}$) of the arm closest to the target (see Fig. 1(b)). Further details of the sensing model can be found in (Wang et al., 2022b, Sec. III-A.).

3. ANALYSIS OF THE NEUROMUSCULAR CONTROL SYSTEM

3.1 Characterizing the rest shape

In this section, we are interested in explaining the curled rest shapes as observed both in attached and isolated arms (Fig. 2(a)), which is suggestive of tonic muscle activity. To incorporate such biological observations within our framework, we first study the equilibrium of the cable equations (4) with a fixed-fixed boundary condition under zero control input ($I^m = 0$).

The equilibrium voltage of the cables must satisfy

$$\lambda^2 V_{ss}^m = V^m + bg(V^m) \quad (6)$$

with fixed-fixed boundary conditions

$$V^m \Big|_{s=0} = V_0^m, \quad V^m \Big|_{s=L} = V_L^m \quad (7)$$

where V_0^m and V_L^m are the fixed voltages for muscle m at the base and at the tip, respectively. Depending on the signs of the boundary voltages, we can explicitly express the equilibrium voltage as presented next.

Lemma 3.1. Consider the voltage equilibrium equation (6) with boundary conditions (7).

a) If $V_0^m V_L^m \geq 0$, then

$$V^m(s) = c_1^m e^{\frac{s}{\lambda}} + c_2^m e^{-\frac{s}{\lambda}} := f(s; c_1^m, c_2^m, \hat{\lambda}) \quad (8)$$

where $c_1^m, c_2^m, \hat{\lambda}$ are constants which depend on V_0^m, V_L^m, λ and b .

b) If $V_0^m V_L^m < 0$, then

$$V^m(s) = \begin{cases} f(s; k_1^m, k_2^m, \hat{\lambda}_1), & 0 \leq s \leq s_1^m \\ f(s; p_1^m, p_2^m, \hat{\lambda}_2), & s_1^m \leq s \leq L \end{cases} \quad (9)$$

where $k_1^m, k_2^m, p_1^m, p_2^m, \hat{\lambda}_1, \hat{\lambda}_2$ are constants which depend on V_0^m, V_L^m, λ and b . Furthermore, the zero-crossing point s_1^m is found by solving the following nonlinear equation

$$f_s(s_1; k_1^m, k_2^m, \hat{\lambda}_1) = f_s(s_1; p_1^m, p_2^m, \hat{\lambda}_2)$$

The proof of Lemma 3.1 is straightforward and utilizes the rectified linear property of the output function $g(\cdot)$. The proof is omitted here due to lack of space.

We next describe how these equilibrium voltages affect the shape of the arm. A straightforward calculation of the statics of (2) with the boundary conditions (3) yields the following expression for equilibrium curvature

$$\kappa(s) = \frac{c(s)}{EI(s)} (\sigma(V^t) - \sigma(V^b)) \quad (10)$$

Once the curvature κ is found, the configuration of the arm is obtained by the virtue of the kinematics (1). The equilibrium shapes are obtained numerically as discussed in Sec. 4.1.

3.2 The reaching problem

In this section, we study the dynamic control problem of designing the input currents $I^m(s, t)$ to drive the arm towards a given static target located at $\mathbf{r}^{\text{target}}$ (Fig. 1(b)). The reaching task is considered completed when the arm stabilizes and either ‘touches’ (target within reach) or ‘points toward’ (target out of reach) the target. A formal definition of these two scenarios are found in (Wang et al., 2022b). In contrast to the fixed-fixed boundary condition for the cable equation (4a) under zero control input for rest state configuration, here we use a free-free boundary condition

$$V_s^m \Big|_{s=0} = V_s^m \Big|_{s=L} = 0 \quad (11)$$

which may be explained by the octopus CNS ‘switching’ from the rest state to the motile state. We next discuss two current control laws.

1) Reference tracking control: Suppose a reference muscle couple control $\bar{u}^m = c(s)\bar{v}^m(s, t)$, $\bar{v}^m \in [0, 1]$, is given which solves the reaching problem. Such a stabilizing control may be obtained by various control methods, e.g. the energy shaping control (Chang et al., 2020, 2021) or feedback control (Wang et al., 2022b). The goal for the neural system is to find current control inputs $I^m(s, t)$ which generate – via the cable dynamics and the neuromuscular coupling – muscle actuations that track the reference couple and effectively stabilize the arm. Here we propose such a control current as

$$I^m = bg(V^m) + (1 - \beta)V^m + \beta\sigma^{-1}(\bar{v}^m) - \lambda^2 (\sigma^{-1}(\bar{v}^m))_{ss} \quad (12)$$

where $\beta > 0$ is a constant. Notice that the activation function $\sigma(\cdot)$ is monotonous so the inverse $\sigma^{-1}(\cdot)$ exists. We refer to the control law (12) as reference tracking control whose stability properties are discussed next.

Proposition 3.1. Suppose the muscular arm (2) is (locally) asymptotically stable under the reference couple control \bar{u}^m . Then, there exists a $\beta > 0$ large enough so that the neuromuscular arm (2, 4, 5) is also (locally) asymptotically stable under the current control (12).

The proof of the proposition relies on separating the time scales of the electrical and mechanical subsystems (Khalil, 2002, Chap. 11.5). A sketch of the proof is given in Appendix A. The benefit of the control law (12) is that any muscle control law can be used as a reference with the neural system being able to track it. However, it is biologically unrealistic to have feedback on the cable voltage. For this reason, we next turn to a more realistic control law.

2) Sensory feedback neural control: Given the sensory information (α, \bar{s}) , we propose a feedback control law at the neural level as

$$\begin{aligned} I(s, t) &= -\mu \sin(\alpha(s, t)) \mathbb{1}\{s \leq \bar{s}(t)\}, \quad \mu > 0 \\ I^t &= -I \mathbb{1}\{I \leq 0\}, \quad I^b = I \mathbb{1}\{I > 0\} \end{aligned} \quad (13)$$

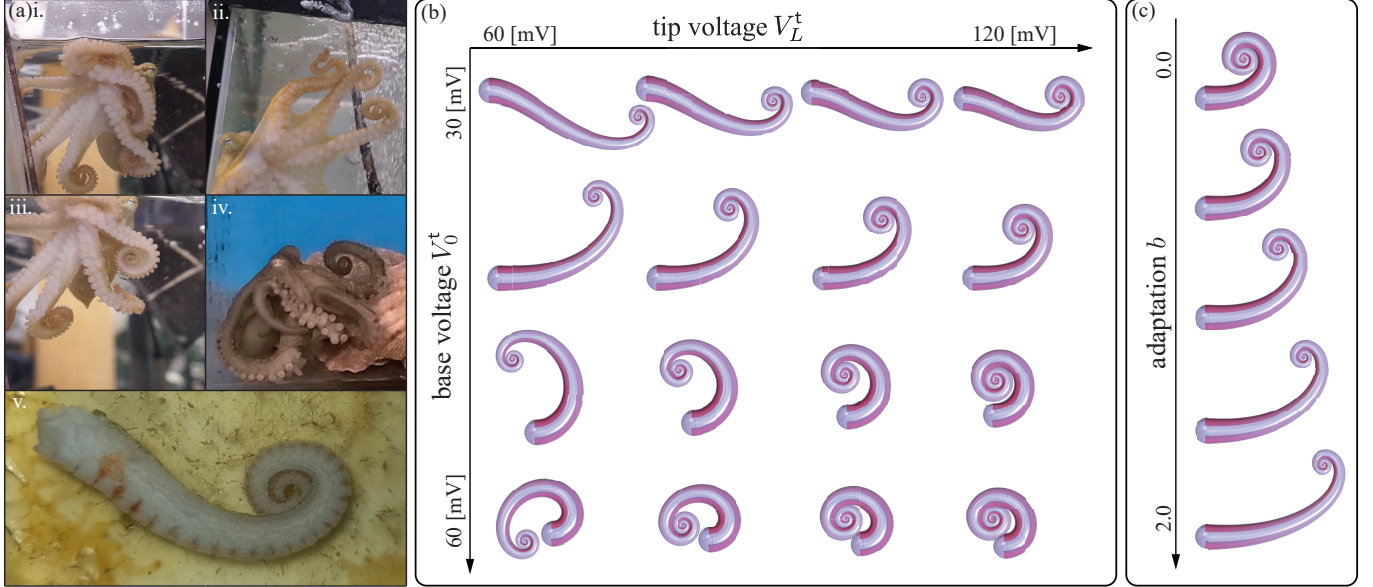


Fig. 2. Curled shapes in both real octopus arms and simulated arms. (a) Snapshots of different octopuses showing curled arm at rest. Subfigures (i.-iv.) are of live octopuses while the subfigure v. is an severed arm that remains curled even after isolation. (b) The equilibrium of the arm under varying base and tip voltages V_0^t and V_L^t for the top longitudinal muscle. The intensities of the distributed muscle actuation are illustrated in red. (c) The equilibrium of the arm under varying adaptation parameter b .

The control law makes the arm active up to the \bar{s} point and passive afterwards. The motivations behind such a feedback control law was the main contribution of our previous work (Wang et al., 2022b). In particular, a central result in (Wang et al., 2022b, Proposition 4.1) states that a couple control law with the same form of the right hand side of (13) achieves the goal of reaching. In this paper, we refer to such a couple control law as the benchmark and denote it by u^* .

Next we discuss the stability properties of the feedback neural control (13).

Proposition 3.2. Consider the dynamics of the neuromuscular arm (2, 4, 5) with the proposed feedback control law (13). Then, there exist a $\mu > 0$ large enough so that the feedback control (13) accomplishes the reaching task.

The proof of this proposition is similar to that of Proposition 3.1 where the sensory feedback control is considered a constant on the fast time-scale of the neural system. The full proof is omitted here on account of space.

4. SIMULATION RESULTS

In this section, we show numerical simulations of an octopus arm equipped with the proposed neuromuscular control architecture. The arm dynamics (2)-(3) are solved using the open-source software *Elastica* (Gazzola et al., 2018; Zhang et al., 2019). In all our simulations, a tapered arm geometry is considered based on measurements in real octopuses (Chang et al., 2020). The neural dynamics (4) are numerically solved consistently with the temporal and spatial discretization of *Elastica* for suitable assimilation. The values of the time constants $\tau, \tilde{\tau}$ are taken in the range identified in (Ekeberg, 1993). The activation function in the neuromuscular coupling equation (5) is chosen as

$$\sigma(V) = \frac{1}{2} \left(1 + \tanh \left(-\frac{1}{40} \operatorname{arctanh}(-0.98(V - 40)) \right) \right) \quad (14)$$

Table 1. Parameters for models and numeric simulation

Parameter	Description	Numerical value
Rod model		
L	length of the undeformed rod [cm]	20
γ^{base}	rod base radius [cm]	1
γ^{tip}	rod tip radius [cm]	0.1
ρ	density [kg/m ³]	1042
ζ	damping coefficient [kg/s]	0.01
E	Young's modulus [kPa]	10
Neuron model		
τ	time constant [s]	0.04
$\tilde{\tau}$	adaptation rate [s]	0.4
λ	length constant [cm]	10

whereas the details of the maximum muscle couple coefficient $c(s)$ in (5) are given in (Chang et al., 2021). The rest of the parameter values used in simulations are reported in Table 1 and further details and explanations are found in (Chang et al., 2020, 2021).

4.1 Rest shape

We obtain the rest state of the arm under zero control input by numerically solving the equilibrium equations (6), (7), (10), and (1), as described in Sec. 3.1. Here we display a collection of rest shapes by varying the boundary voltage values (V_0^m, V_L^m) and the adaptation parameter b .

We first fix the boundary voltages $V_0^b = 40$ [mV] and $V_L^b = 0$ [mV] for the bottom longitudinal muscle. Then, two sets of experiments are carried out.

1) *Varying the top boundary voltages:* We fix the adaptation parameter $b = 1.0$ and vary the boundary voltages V_0^t and V_L^t for the top longitudinal muscle by taking their values from the sets $\{30, 40, 50, 60\}$ [mV] and $\{60, 80, 100, 120\}$ [mV],

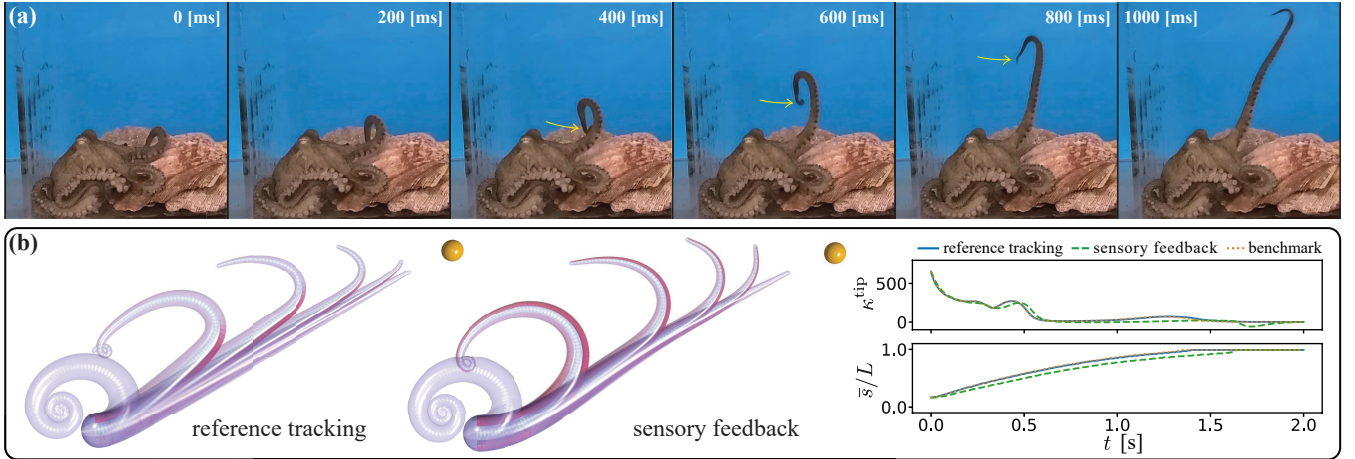


Fig. 3. (a) A video sequence of an *Octopus bimaculoides* performing bend propagation. Yellow arrows indicate the initial curling at the tip which gradually vanishes during the bend propagation movement. (b) The rod is initialized with a bend at the base and the curl at the tip. The first and second columns are simulation results of rod reaching towards a static target under reference tracking control and sensory feedback control, respectively. The third column is the κ^{tip} and \bar{s} trajectories comparison among reference tracking control (blue solid lines), sensory feedback control (green dash lines), and the benchmark control (orange dotted lines).

respectively. This results in a 4-by-4 chart as illustrated in Fig. 2(b). We observe that as V_0^t increases (columns), the arm tends to bend more at the base. On the other hand, as V_L^t increases (rows), the tip curls more. Some of the simulated rest shapes present a good qualitative match with the recordings from real octopuses. For instance, the shape in row-2/column-4 matches Fig. 2(a)i.-iii., where the arm is straight near the base and curls up at the tip. Similarly, the row-4/column-2 result shows a tip curling with a bent base, matching the recording Fig. 2(a)iv. Finally, row-1/column-4 presents a shape similar to the isolated curled arm of Fig. 2(a)v.

2) *Varying the adaptation parameter*: We fix the base and tip voltage of the top longitudinal muscle to $V_0^t = 40$ [mV] and $V_L^t = 80$ [mV]. Then, we vary the adaptation parameter b from the set $\{0, 0.5, 1.0, 1.5, 2.0\}$ and show the resulting rest shapes in Fig. 2(c). We see that as the adaptation increases, the arm tends to unwind, or in other words, the arm curls less. Mathematically speaking, adaptation parameter b takes effect in changing the equivalent length constant $\tilde{\lambda} = \frac{\lambda}{\sqrt{b+1}}$. Higher adaptation results in smaller equivalent length constant, hence giving equilibrium voltage solution with faster decaying.

4.2 Reaching maneuver

Here we demonstrate goal-directed arm movements as a solution to the reaching problem described in Sec. 3.2. For this experiment, the arm is initialized at the equilibrium configuration under voltage boundary values $V_0^t = 65$ [mV], $V_L^t = 65$ [mV], $V_0^b = 40$ [mV], $V_L^b = 0$ [mV], and the adaptation parameter $b = 1.0$. This initial configuration corresponds to row-4/column-2 shape in Fig. 2(b). A static target at coordinates $[0.2, 0.1]$ [m], outside the arm's reach, is presented. The control gains $\beta = 10$ and $\mu = 500$ are chosen for reference tracking control law (12) and sensory feedback control law (13), respectively. For reference tracking, the benchmark control u^* is chosen as the reference. In Fig. 3(b), we illustrate arm simulations under both reference tracking control (12) and sensory feedback neural control (13). As we can see from the snapshots of the

dynamic simulation in Fig. 3(b), both control laws push the initial bend towards the target until the arm eventually stabilizes in a configuration pointing towards the target.

Additionally, we illustrate two properties of the arm: (i) tip curvature $\kappa^{\text{tip}}(t)$ which is defined to be the average curvature of the final 10% of the arm $\kappa^{\text{tip}}(t) := \frac{1}{0.1L} \int_{0.9L}^L \kappa(s, t) ds$, and (ii) $\bar{s}(t)/L$. The \bar{s} point can be approximately regarded as the position of the propagating bend during the reaching movement. We see from the trajectories of κ^{tip} in Fig. 3(b) that the initial tip curling is released, qualitatively matching bend propagation recordings from biological experiments (Fig. 3(a)). Besides κ^{tip} , the trajectories of \bar{s}/L also show that the reference tracking control successfully tracks the reference.

5. CONCLUSION

In this paper, a model for the octopus peripheral nervous system is proposed and integrated within a muscular soft arm. For the proposed neuromuscular control architecture, several analytical results are provided including the characterization of the equilibrium at rest states, and its analytical expression. Numerical results show a qualitative match with experimental observations of curled octopus arms at rest. Besides the rest state, active arm motions are also computationally demonstrated for two proposed control laws. The stability of the closed-loop system under the proposed control laws is discussed. The performance of the two control laws are numerically compared against a benchmark control previously derived. Future work includes investigating possible wave solutions to the neural dynamics, and studying whether mutual inhibition among muscles exist and how it affects the behavior of the arm.

ACKNOWLEDGEMENTS

The authors are thankful to Dr. Rhanor Gillette's lab at the University of Illinois and Dr. William Gilly's lab at the Hopkins Marine Station, Stanford University, where the octopus experiments were performed.

REFERENCES

- Antman, S.S. (1995). *Nonlinear Problems of Elasticity*. Springer.
- Audu, M. and Davy, D. (1985). The influence of muscle model complexity in musculoskeletal motion modeling.
- Aydin, O., Zhang, X., Nuethong, S., Pagan-Diaz, G.J., Bashir, R., Gazzola, M., and Saif, M.T.A. (2019). Neuromuscular actuation of biohybrid motile bots. *Proceedings of the National Academy of Sciences*, 116(40), 19841–19847.
- Cacace, S., Lai, A.C., and Loreti, P. (2019). Control strategies for an octopus-like soft manipulator. In *ICINCO (1)*, 82–90.
- Chang, H.S., Halder, U., Gribkova, E., Tekinalp, A., Naughton, N., Gazzola, M., and Mehta, P.G. (2021). Controlling a cyberoctopus soft arm with muscle-like actuation. In *2021 60th IEEE Conference on Decision and Control (CDC)*, 1383–1390. IEEE.
- Chang, H.S., Halder, U., Shih, C.H., Naughton, N., Gazzola, M., and Mehta, P.G. (2022). Energy shaping control of a muscular octopus arm moving in three dimensions. *arXiv preprint arXiv:2209.04089*.
- Chang, H.S., Halder, U., Shih, C.H., Tekinalp, A., Parthasarathy, T., Gribkova, E., Chowdhary, G., Gillette, R., Gazzola, M., and Mehta, P.G. (2020). Energy shaping control of a cyberoctopus soft arm. In *2020 59th IEEE Conference on Decision and Control (CDC)*, 3913–3920. IEEE.
- Di Clemente, A., Maiole, F., Bornia, I., and Zullo, L. (2021). Beyond muscles: role of intramuscular connective tissue elasticity and passive stiffness in octopus arm muscle function. *Journal of Experimental Biology*, 224(22), jeb242644.
- Ekeberg, Ö. (1993). A combined neuronal and mechanical model of fish swimming. *Biological cybernetics*, 69(5), 363–374.
- FitzHugh, R. (1961). Impulses and physiological states in theoretical models of nerve membrane. *Biophysical journal*, 1(6), 445–466.
- Folgheraiter, M., Keldibek, A., Aubakir, B., Gini, G., Franchi, A.M., and Bana, M. (2019). A neuromorphic control architecture for a biped robot. *Robotics and Autonomous Systems*, 120, 103244.
- Gazzola, M., Dudte, L., McCormick, A., and Mahadevan, L. (2018). Forward and inverse problems in the mechanics of soft filaments. *Royal Society Open Science*, 5(6), 171628.
- Grasso, F.W. (2014). The octopus with two brains: how are distributed and central representations integrated in the octopus central nervous system. *Cephalopod cognition*, 94–122.
- Graziadei, P. and Gagne, H. (1976). Sensory innervation in the rim of the octopus sucker. *Journal of morphology*, 150(3), 639–679.
- Gutfreund, Y., Flash, T., Fiorito, G., and Hochner, B. (1998). Patterns of arm muscle activation involved in octopus reaching movements. *Journal of Neuroscience*, 18(15), 5976–5987.
- Gutnick, T., Zullo, L., Hochner, B., and Kuba, M.J. (2020). Use of peripheral sensory information for central nervous control of arm movement by octopus vulgaris. *Current Biology*, 30(21), 4322–4327.
- Hanassy, S., Botvinnik, A., Flash, T., and Hochner, B. (2015). Stereotypical reaching movements of the octopus involve both bend propagation and arm elongation. *Bioinspiration & biomimetics*, 10(3), 035001.
- Hatze, H. (1977). A myocybernetic control model of skeletal muscle. *Biological cybernetics*, 25(2), 103–119.
- Hodgkin, A.L. and Huxley, A.F. (1952). A quantitative description of membrane current and its application to conduction and excitation in nerve. *The Journal of physiology*, 117(4), 500.
- Ijspeert, A.J., Crespi, A., Ryczko, D., and Cabelguen, J.M. (2007). From swimming to walking with a salamander robot driven by a spinal cord model. *science*, 315(5817), 1416–1420.
- Izhikevich, E.M. (2007). *Dynamical systems in neuroscience*. MIT press.
- Kennedy, E.L., Buresch, K.C., Boinapally, P., and Hanlon, R.T. (2020). Octopus arms exhibit exceptional flexibility. *Scientific reports*, 10(1), 1–10.
- Khalil, H.K. (2002). *Nonlinear systems third edition*. Patience Hall.
- Kier, W.M. (2016). The musculature of coleoid cephalopod arms and tentacles. *Frontiers in cell and developmental biology*, 4, 10.
- Kier, W.M. and Stella, M.P. (2007). The arrangement and function of octopus arm musculature and connective tissue. *Journal of morphology*, 268(10), 831–843.
- Koch, C. (1984). Cable theory in neurons with active, linearized membranes. *Biological cybernetics*, 50(1), 15–33.
- Levy, G., Neshet, N., Zullo, L., and Hochner, B. (2017). Motor control in soft-bodied animals: the octopus. In *The Oxford Handbook of Invertebrate Neurobiology*.
- Liu, G.L., Habib, M.K., Watanabe, K., and Izumi, K. (2008). Central pattern generators based on matsuoka oscillators for the locomotion of biped robots. *Artificial Life and Robotics*, 12(1), 264–269.
- Mather, J. (2021). Octopus consciousness: the role of perceptual richness. *NeuroSci*, 2(3), 276–290.
- Mather, J.A. (1998). How do octopuses use their arms? *Journal of Comparative Psychology*, 112(3), 306.
- Matsuoka, K. (1984). The dynamic model of binocular rivalry. *Biological cybernetics*, 49(3), 201–208.
- Matzner, H., Gutfreund, Y., and Hochner, B. (2000). Neuromuscular system of the flexible arm of the octopus: physiological characterization. *Journal of neurophysiology*, 83(3), 1315–1328.
- Nagumo, J., Arimoto, S., and Yoshizawa, S. (1962). An active pulse transmission line simulating nerve axon. *Proceedings of the IRE*, 50(10), 2061–2070.
- Neshet, N., Levy, G., Zullo, L., and Hochner, B. (2020). Octopus motor control. *Oxford Research Encyclopedia of Neuroscience*. Oxford University Press, USA.
- Neshet, N., Maiole, F., Shomrat, T., Hochner, B., and Zullo, L. (2019). From synaptic input to muscle contraction: arm muscle cells of octopus vulgaris show unique neuromuscular junction and excitation–contraction coupling properties. *Proceedings of the Royal Society B*, 286(1909), 20191278.
- Packard, A. and Sanders, G.D. (1971). Body patterns of octopus vulgaris and maturation of the response to disturbance. *Animal Behaviour*, 19(4), 780–790.
- Polykretis, I., Supic, L., and Danielescu, A. (2022). Bioinspired smooth neuromorphic control for robotic arms. *arXiv preprint arXiv:2209.02787*.
- Rall, W. (1962). Theory of physiological properties of dendrites. *Annals of the New York Academy of Sciences*, 96(4), 1071–1092.
- Rowell, C.F. (1963). Excitatory and inhibitory pathways in the arm of octopus. *Journal of Experimental Biology*, 40(2), 257–270.

- Sfakiotakis, M. and Tsakiris, D.P. (2007). Neuromuscular control of reactive behaviors for undulatory robots. *Neurocomputing*, 70(10-12), 1907–1913.
- Sumbre, G., Gutfreund, Y., Fiorito, G., Flash, T., and Hochner, B. (2001). Control of octopus arm extension by a peripheral motor program. *Science*, 293(5536), 1845–1848.
- Tian, J. and Lu, Q. (2015). Simulation of octopus arm based on coupled cpgs. *Journal of Robotics*, 2015.
- Tuckwell, H.C. (1988). *Introduction to theoretical neurobiology*. New York: Cambridge University Press.
- Wang, T., Halder, U., Chang, H.S., Gazzola, M., and Mehta, P.G. (2021). Optimal control of a soft cyberoctopus arm. In *2021 American Control Conference (ACC)*, 4757–4764. IEEE.
- Wang, T., Halder, U., Gribkova, E., Gazzola, M., and Mehta, P.G. (2022a). Control-oriented modeling of bend propagation in an octopus arm. In *American Control Conference (ACC)*, 1359–1366. IEEE.
- Wang, T., Halder, U., Gribkova, E., Gillette, R., Gazzola, M., and Mehta, P.G. (2022b). A sensory feedback control law for octopus arm movements. In *2022 61th IEEE Conference on Decision and Control (CDC) (accepted)*. IEEE.
- Wang, T., Taghvaei, A., and Mehta, P.G. (2020). Bio-inspired learning of sensorimotor control for locomotion. In *2020 American Control Conference (ACC)*, 2188–2193. IEEE.
- Wells, M.J. (1978). *Octopus: physiology and behaviour of an advanced invertebrate*. Springer.
- Yekutieli, Y., Sagiv-Zohar, R., Aharonov, R., Engel, Y., Hochner, B., and Flash, T. (2005a). Dynamic model of the octopus arm. i. biomechanics of the octopus reaching movement. *Journal of neurophysiology*, 94(2), 1443–1458.
- Yekutieli, Y., Sagiv-Zohar, R., Hochner, B., and Flash, T. (2005b). Dynamic model of the octopus arm. ii. control of reaching movements. *Journal of neurophysiology*, 94(2), 1459–1468.
- Yoram, Y., German, S., Tamar, F., and Binyamin, H. (2002). How to move with no rigid skeleton? the octopus has the answers. *Biologist*, 49(6), 250–254.
- Young, J.Z. (1971). *The anatomy of the nervous system of Octopus vulgaris*. Oxford: Clarendon Press.
- Zhang, X., Chan, F.K., Parthasarathy, T., and Gazzola, M. (2019). Modeling and simulation of complex dynamic musculoskeletal architectures. *Nature Communications*, 10(1), 1–12.

Appendix A. SKETCH OF PROOF OF PROPOSITION 3.1

We first separate the time-scales of the muscular arm dynamics 2 and the neural dynamics 4 by noting that the neural system is ‘fast’ because of the small time constants $\tau, \tilde{\tau}$ (also verified numerically). The ‘slow’ mechanical system can be regarded as frozen with respect to the fast electrical system. Then, the Proposition 3.1 is proved by using the method of singular perturbation, as developed in (Khalil, 2002, Chap. 11).

Here we give a sketch of the proof by providing various necessary steps. Also, we remove the superscripts m for notational ease. Furthermore, we assume the reference muscle control is a constant in time, i.e. $\bar{u}(s) = c(s)\bar{v}(s)$. Denote the resulting reference voltage as $\bar{V} = \sigma^{-1}(\bar{v})$. Then we have the following result.

Lemma A.1. Consider the neural dynamics (4) with the current control (12), where the reference is constant in time. Then

the closed loop neural dynamics is exponentially stable at the equilibrium $(\bar{V}, bg(\bar{V}))$.

Proof: We propose the following Lyapunov candidate for the closed loop neural system

$$\mathcal{E}_0(V, W) = \frac{1}{2} \int_0^L \tau (V - \bar{V})^2 + \tilde{\tau} (W - bg(\bar{V}))^2 ds$$

It can be readily derived that

$$\begin{aligned} \frac{d\mathcal{E}_0}{dt} &= \int_0^L -\beta (V - \bar{V})^2 - (W - bg(\bar{V}))^2 - (V - \bar{V})(W - bg(\bar{V})) \\ &\quad + b(V - \bar{V} + W - bg(\bar{V}))(g(V) - g(\bar{V})) \\ &\quad + \lambda^2 (V - \bar{V})(V_{ss} - \bar{V}_{ss}) ds \\ &\leq \int_0^L -(\beta - b)|V - \bar{V}|^2 - |W - bg(\bar{V})|^2 \\ &\quad + (b+1)|V - \bar{V}||W - bg(\bar{V})| - |V_s - \bar{V}_s|^2 ds \end{aligned}$$

If β satisfies $\beta > \frac{(b+1)^2}{4} + b$, we have $\frac{d\mathcal{E}_0}{dt} \leq 0$ and is only equal to zero at the equilibrium $(\bar{V}, bg(\bar{V}))$. Therefore, the equilibrium is (locally) asymptotically stable.

Furthermore, for a constant $k = \frac{1}{\tilde{\tau}}$, if $\beta > \frac{(b+1)^2}{2} + b + \frac{k\tau}{2}$, we have

$$\frac{d\mathcal{E}_0}{dt} \leq -k\mathcal{E}_0$$

and thus the equilibrium is proved to be exponentially stable.

Next, we turn to the mechanical system. It has been shown in (Chang et al., 2021) that if the internal muscle couple \bar{u} is a constant, then it is expressible as gradients of an energy function called *muscle stored energy function*). As a consequence, the system maintains its Hamiltonian structure (with damping) and (locally) asymptotic convergence to an equilibrium can be readily shown. The closed-loop Hamiltonian can be taken as a Lyapunov functional, here denoted as \mathcal{H} . From (Chang et al., 2021, Proposition 4.1), we have that $\frac{d\mathcal{H}}{dt} \leq -\zeta \int_0^L \left| \frac{1}{\rho I} p \right|^2 ds$ where $p = \rho I \dot{\theta}_t$ is the angular momentum.

Now, let us consider the following Lyapunov candidate for the coupled system (2, 4, 5, 12) as $\mathcal{E} = \mathcal{E}_0 + \mathcal{H}$. Then along the trajectories of the coupled system, we have

$$\frac{d\mathcal{E}}{dt} = \frac{d\mathcal{E}_0}{dt} + \int_0^L \frac{1}{\rho I} p \left(-\frac{\zeta}{\rho I} p + (\sigma(V) - u)_s \right) ds$$

The third term is the extra term due to the coupling of the two subsystems. Suppose the model parameters are such that the following inequality holds

$$\left| \int_0^L \frac{1}{\rho I} p (\sigma(V) - u)_s ds \right| \leq \beta_0 \int_0^L \frac{1}{\rho I} |p| |V - \bar{V}| ds$$

for some constant $\beta_0 > 0$. Then, we have

$$\begin{aligned} \frac{d\mathcal{E}}{dt} &\leq \int_0^L -\zeta \left| \frac{1}{\rho I} p \right|^2 - \frac{k\tau}{2} |V - \bar{V}|^2 + \beta_0 \left| \frac{1}{\rho I} p \right| |V - \bar{V}| \\ &\quad - \frac{k\tilde{\tau}}{2} |W - bg(\bar{V})|^2 - |V_s - \bar{V}_s|^2 ds \end{aligned}$$

Thus we finally obtain $\frac{d\mathcal{E}}{dt} \leq 0$ for $\beta_0^2 \leq 2\zeta k\tau$. Furthermore, $\frac{d\mathcal{E}}{dt} = 0$ only at the equilibrium of the coupled system. Hence, we proved that the coupled system is also (locally) asymptotically stable at the equilibrium.